Biochimica et Biophysica Acta 1833 (2013) 2714–2724

Contents lists available at ScienceDirect

Biochimica et Biophysica Acta

journal homepage: www.elsevier.com/locate/bbamcr

Protein aggregation propensity is a crucial determinant of intracellular inclusion formation and quality control degradation

Anna Villar-Piqué, Salvador Ventura *

Departament de Bioquímica i Biologia Molecular, Facultat de Biociències, Universitat Autònoma de Barcelona, E-08193 Bellaterra, Spain
Institut de Biotecnologia i de Biomedicina, Universitat Autònoma de Barcelona, E-08193 Bellaterra, Spain

ARTICLE INFO

Article history:
Received 14 May 2013
Received in revised form 21 June 2013
Accepted 24 June 2013
Available online 12 July 2013

Keywords:
Protein aggregation
Protein folding
Amyloid peptide
Fluorescent reporter
Protein degradation
Yeast

ABSTRACT

Protein aggregation is linked to many pathological conditions, including several neurodegenerative diseases. The aggregation propensities of proteins are thought to be controlled to a large extent by the physicochemical properties encoded in the primary sequence. We have previously exploited a set of amyloid β peptide (Aβ42) variants exhibiting a continuous gradient of intrinsic aggregation propensities to demonstrate that this rule applies in vivo in bacteria. In the present work we have characterized the behavior of these Aβ42 mutants when expressed in yeast. In contrast to bacteria, the intrinsic aggregation propensity is gated by yeast, in such a way that this property correlates with the formation of intracellular inclusions only above a specific aggregation threshold. Proteins displaying solubility levels above this threshold escape the inclusion formation pathway. In addition, the most aggregation-prone variants are selectively cleared by the yeast quality control degradation machinery. Thus, both inclusion formation and proteolysis target the same aggregation-prone variants and cooperate to minimize the presence of these potentially dangerous species in the cytosol. The demonstration that sorting to these pathways in eukaryotes is strongly influenced by protein primary sequence should facilitate the development of rational approaches to predict and hopefully prevent in vivo protein deposition.

1. Introduction

Protein aggregation and the long term cellular persistence of aggregates are pathological hallmarks of a large set of human disorders, the so-called conformational diseases, such as Alzheimer's (AD), Huntington's (HD) and Parkinson's (PD) diseases, and diabetes type II or transmissible spongiform encephalopathies [1,2]. Moreover, protein deposition is also a common phenomenon during recombinant expression in simple organisms such as unicellular fungi or bacteria [3,4]. Interestingly, the aggregates formed in these microorganisms resemble those involved in the onset of the aforementioned disorders [5–7], indicating that protein self-assembly into β-sheet enriched amyloid-like structures is a generic process in direct competition with native protein folding [8–10], regardless of the considered host. Indeed, it has been shown that the large majority of polypeptides display at least one and often multiple aggregation-prone regions, usually involved in the formation of the hydrophobic core [11,12]. As it occurs with folding, the aggregation propensity of proteins represents an essential property of the behavior of polypeptides encoded in their primary sequences [13–15]. Different bioinformatic algorithms have exploited this feature to predict protein deposition and amyloid formation by identifying and quantifying aggregation-promoting regions within a given sequence [16–19]. Despite their success in predicting in vitro aggregation, the challenge is asserting if the predictive power of these programs also applies in a more complex biological context [16]. Addressing this question is not trivial, since quantitative evaluation of the aggregation propensities of polypeptides in vivo is technically complex. In a first step toward this direction, we exploited in previous works the competition between protein folding and aggregation in the bacterial cytosol to approximate intracellular aggregation rates. Essentially, we generated 19 variants of the Aβ peptide (Aβ42) in which the original Phe residue in position 19 was substituted by the rest of natural proteinogenic amino acids. This residue is located in the central hydrophobic cluster (CHC), a short stretch comprising residues from Leu17 to Ala21 that controls, to a large extent, the aggregation propensity of the entire sequence. The 20 Aβ42 mutants were fused to the green fluorescent protein (GFP), which acts as a reporter of the aggregation propensity of the Aβ moiety and were recombinantly expressed in *Escherichia coli*. The expression of the different peptide variants in *E. coli* resulted in the formation of cytoplasmic amyloid-like inclusion bodies whose

Abbreviations: Aβ42, 42 residue-length amyloid β peptide; AD, Alzheimer's disease; ATG1, autophagy-specific gene 1; cfu, colony-forming units; CHC, central hydrophobic cluster; DMSO, dimethyl sulfoxide; EtOH, ethanol; GFP, green fluorescent protein; HD, Huntington's disease; PD, Parkinson's disease; PMSF, phenylmethanesulfonyl fluoride; PQC, protein quality control machinery; SC-URA, synthetic complete medium deficient for uracil

* Corresponding author at: Institut de Biotecnologia i de Biomedicina, Universitat Autònoma de Barcelona, E-08193 Bellaterra, Spain. Tel.: +34 93 586 8956.
E-mail address: salvador.ventura@uab.es (S. Ventura).

0167-4889/$ – see front matter © 2013 Elsevier B.V. All rights reserved.
http://dx.doi.org/10.1016/j.bbamcr.2013.06.023

GFP activity reflected the aggregation rate of the corresponding mutant [20,21]. These data constitute the core of AGGRESCAN, a method implemented in our group to predict protein aggregation propensity [22,23]. We have shown recently that in this model system the cellular fitness cost induced by protein deposition is tightly regulated by the intrinsic properties of the polypeptide chain, linking thus phenotype and sequence [24,25].

We have applied here the same approach in yeast to provide a quantitative assessment of the aggregation properties of proteins and how they correlate with sequential features in a more complex eukaryotic background. The budding yeast *Saccharomyces cerevisiae* is an excellent model system for the study of human cell biology in health and disease, since the basic features of eukaryotic cell biology evolved before the split between yeast and metazoans. This organism shares with higher eukaryotes numerous fundamental cellular pathways involved in neurodegeneration, such as protein quality control, membrane trafficking, autophagy or oxidative stress [26,27]. On this regard, humanized yeast models for AD, HD and PD have been successfully developed, recapitulating some of the pathological features associated with these disorders [28–34]. Here we analyzed the aggregation properties of the above mentioned Aβ42 mutants when expressed in yeast. In contrast to bacteria, where degradative pathways did not seem to affect the fate of these polypeptides, in yeast Aβ42 variants are actively cleared from the cytosol by the yeast protein quality control machinery. The intrinsic properties of the peptides determine both their in vivo intracellular aggregation and degradation. This model system should allow to rationalize and predict the impact of sequential changes in the deposition and degradation of amyloidogenic polypeptides in eukaryotic environments.

2. Material and methods

2.1. Yeast strain and plasmids

Yeast strain BY4741 (*MAT* a *his*3Δ1 *leu*2Δ0 *met*15Δ0 *ura*3Δ0) was transformed with pESC(-Ura) plasmids (Stratagene), encoding for the Aβ42–GFP fusion protein and the 19 variants differing in the 19th residue of Aβ42, as previously described [3]. Standard lithium/polyethylene glycol protocol was used for the transformation and a glucose selective synthetic complete medium deficient for uracil (SC-URA) was employed for plasmid selection.

2.2. Protein expression

Yeast cells were grown overnight in glucose SC-URA medium at 30 °C and 100 μL was used to inoculate 5 mL of fresh medium. At an OD_{600} of 0.5, cells were changed to a fresh raffinose SC-URA medium. After 30 min, cells were changed again to a fresh SC-URA medium containing 2% of galactose as a source of carbon to induce the recombinant protein expression. After 15 h at 30 °C, cells were harvested, washed in sterile water and pellets were stored at −80 °C for further analysis.

2.3. Microscopy

Cells were washed three times with sterile PBS and 5 μL was placed on top of microscopy glass slides and covered with coverslips. Images were obtained at a 40-fold magnification using an emission filter for GFP under UV light excitation in a Leica fluorescence microscope (Leica DMBR, Heidelberg, Germany).

2.4. Fluorescence measurements

Cell pellets were resuspended in PBS to an OD_{600} of 1. The emission spectra of GFP were recorded on a Cary Eclipse Spectrofluorometer (Agilent Technologies, Santa Clara, CA, USA) in the range 500–600 nm with a data interval of 1 nm and using an excitation wavelength of 488 nm. The experiments were carried out in triplicates.

2.5. Immunoblotting analysis

Cell pellets were resuspended in PBS. 200 μL of each mutant was prepared to an OD_{600} of 20 and 5 μL was used for total fraction Western-blots. For soluble/insoluble fraction analysis, 100 μL was centrifuged and resuspended in the same volume of Y-PER protein extraction reagent from Thermo Scientific (supplemented with a protease inhibitor cocktail tablet) to induce cell lysis. After 20 min of incubation at room temperature under mild agitation, mixtures were centrifuged at maximum speed for 30 min. Insoluble fractions were resuspended in 100 μL of PBS containing a protease inhibitor cocktail tablet and used for Western-blot analysis, together with 100 μL of the soluble fraction. 5 μL of each sample was loaded in a 14% SDS-PAGE and blotted onto a PVDF membrane. Immunodetection was performed using β-amyloid antibody 6E10 from Covance and membranes were developed with the ECL method. Densitometries were performed using ImageJ software. The experiments were carried out in triplicates.

2.6. Flow cytometry analysis

Cells expressing Aβ42*wt*–GFP and Aβ42F19E–GFP were harvested and washed three times in 0.22 μm filtered PBS. Flow cytometry measurements were performed using a FACSCanto flow cytometer (BD Biosciences, San Jose, CA, USA) equipped with a 488 nm blue argon laser. Gated cells (by means of FSC and SSC parameters) were analyzed for green emission measured on a 530/30 nm BP filter. Obtained data were analyzed using BD FACSDiva 4.0 software.

2.7. Cell viability assays

Overnight cultures of Aβ42*wt*–GFP and Aβ42F19E–GFP grown in SC-URA medium supplied with glucose (or galactose, for colony-forming units assay) were washed with sterile water and diluted to an OD_{600} of 0.8. The experiments were carried out in triplicates.

For determining the colony-forming units per mL (cfu/mL), 100 μL of serial dilutions (10^{-3}–10^{-7}) was plated in medium supplied with glucose and galactose and incubated at 30 °C for 3 days. Only plates containing between 30 and 300 colonies were monitored.

For spotting assays, 8 μL of serial dilutions (10^{-1}–10^{-4}) was spotted in glucose and galactose plates, subsequently incubated at 30 °C for 2 days. This experiment was carried out with all Aβ42–GFP mutants.

For growth curves, overnight cultures diluted in water were used to inoculate 250 μL of fresh medium containing glucose and galactose to a final OD_{600} of 0.15 in 96 well plates. Culture growth was monitored overnight at 28 °C in a Victor 3 Plate Reader (Perkin-Elmer, Inc., Waltham, MA, USA) measuring the OD_{595} every 15 min.

2.8. Proteolytic degradation analysis

Yeast strains specifically used in these assays were: BJ5459 (*MAT* a *ura*3-52 *trp*1 *lys*2-801 *leu*2Δ1 *his*3Δ200 *pep*4Δ::*HIS*3 *prb*1Δ1.6R *can*1 GAL) [35], and Δ*erg6* and Δ*atg1*, both in BY4741 background.

In experiments with chemical compounds, the cell wall permeable yeast strain, Δ*erg6*, transformed with pESC(-Ura) plasmids, was incubated overnight with galactose SC-URA medium. Prior to drug application, protein expression was arrested by changing medium from galactose to glucose supplemented. Incubation with drugs was performed for 4 h at 30 °C. The chemical compounds and the final concentrations used in these assays were: phenylmethanesulfonyl fluoride (PMSF) dissolved in ethanol (EtOH) at 1 mM, rapamycin dissolved in dimethyl sulfoxide (DMSO) at 100 nM and MG-132 dissolved in DMSO at 50 μM; all of them from Sigma-Aldrich. EtOH and DMSO

treatments at the corresponding concentrations were used as controls. The experiments were carried out in triplicates.

3. Results

3.1. Prediction of the aggregation propensity of the 20 Aβ42 mutants

The library of 20 Aβ42 mutants used in this study differs only in the residue in position 19 of the Aβ peptide [20]. This residue is a Phe in the wild type sequence, is located in the CHC of the peptide and has been shown to affect the folding, self-assembly, and fibril structure of Aβ [36,37]. We analyzed the aggregation propensity of these variants with three different algorithms conceptually unrelated to AGGRESCAN [22] to obtain an unbiased evaluation of their intrinsic aggregation properties previous to their experimental characterization in yeast. We employed: (i) Zyggregator [38], which uses a set of physicochemical properties of amino acid residues such as hydrophobicity, charge, and the propensity to adopt α-helical or β-structural conformations. (ii) FoldAmyloid [39], which exploits the amino acid expected packing density and their propensity to establish hydrogen bonds and (iii) TANGO [40], which is based on the tendency of a sequence to form β-sheets that will remain buried in the structure of an amyloid. The aggregation properties predicted by these algorithms, as well as AGGRESCAN, for the 20 Aβ42 mutants were normalized and they are compared in Fig. 1. All predictors converge on ascribing the higher propensity values to Aβ42 variants displaying aromatic and hydrophobic residues (Ile, Leu, Met, Phe, Val, Trp and Tyr) in position 19.

3.2. Formation of aggregated foci by Aβ42–GFP mutants in the yeast cytoplasm

Following the same strategy that we used previously in bacteria, the 20 Aβ42 mutants were fused to GFP and the resulting fusions (Aβ–GFP) were expressed individually in the BY4741 yeast strain. We placed Aβ–GFP under control of the tightly regulated galactose-inducible *GAL1* promoter to allow, rapid, strong and synchronous induction of protein expression in all cells. After 15 h of protein expression, GFP fluorescence was visible in the cytoplasm of all the strains. However, fluorescent foci were only observable in cells expressing certain mutants, while the rest of the variants presented diffuse GFP fluorescence throughout the cytoplasm (Fig. 2A). We monitored and quantified the presence of foci in 1000 yeast cells for each of the 20 Aβ–GFP variants (Fig. 2B). Ile, Phe, Tyr, Leu, Met, Trp and Val mutants displayed the higher proportion of cells containing one or more foci in their cytoplasm, followed by Cys, Ala and, to a lower extent, Thr. The rest of variants did not exhibit any detectable Aβ–GFP foci, which contrasts with mutants like Ile or Phe, where more than 60% of the cells contained visible aggregates (Fig. 2B). According to the predictions in the previous section, the mutants resulting in the formation of foci in the yeast cytoplasm correspond to those exhibiting a high intrinsic aggregation propensity. We explored if for those mutants there exists any correlation between the number of cells displaying visible aggregates and the previously calculated relative aggregation rates in the bacterial cytosol (Fig. 2C). A striking correlation between these two parameters was observed ($R = 0.95$, $p < 0.00005$), suggesting that the formation of protein inclusions occurs under similar constraints in bacteria and yeast cytosols. The data also imply the presence of an aggregation threshold below which no foci are formed. The residues leading to the formation of foci correspond precisely with the 10 more aggregation-prone amino acids in the AGGRESCAN scale, in such a way that mutants with residues whose intrinsic aggregation propensities are below that of Thr do not result in any foci formation. Fitting the data with the other aggregation propensity scales resulted in lower correlations (Fig. S1), indicating that the aggregation propensities in yeast, in terms of foci formation, essentially recapitulate those observed in bacteria.

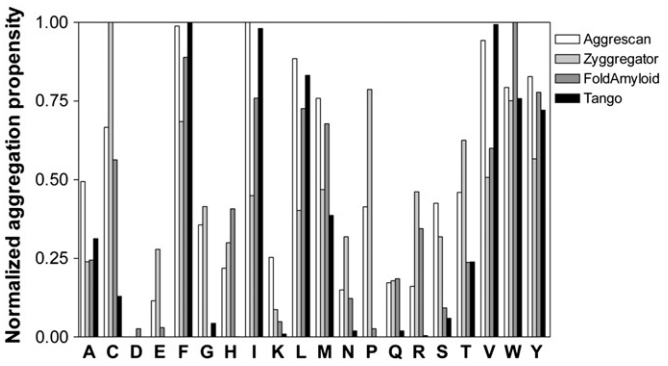

Fig. 1. Comparison of the predicted aggregation propensities of the 20 Aβ42 mutants. Bar graph representing the aggregation propensities obtained by means of four bioinformatic algorithms: AGGRESCAN (http://bioinf.uab.es/aggrescan/), Zyggregator (http://www-vendruscolo.ch.cam.ac.uk/zyggregator.php), FoldAmyloid (http://bioinfo.protres.ru/fold-amyloid/oga.cgi) and TANGO (http://tango.crg.es/). Values have been normalized for each predictor.

In order to test if the formation of foci was associated with a cytotoxic effect, we performed spotting assays for the 20 different mutants in the presence of glucose (repressing conditions) and galactose (inducing conditions). The data for selected mutants displaying increasing aggregation propensity are shown in Fig. 2D and the complete dataset in Fig. S2. No significant differences between mutants could be observed. These results are in good agreement with previous data obtained for fusions of Aβ42 variants displaying different aggregation propensities in frame with GFP [29] or with the functional domain of Sup35 [41]. We also monitored the growth kinetics of Phe and Glu mutants, as representative of inclusion-forming and inclusion-free variants, respectively, under repressing and inducing conditions. As expected, yeast growth in glucose-containing medium was faster than in the presence of galactose, however we could not observe significant differences in growth rates between mutants in any of the two conditions (Fig. S3). The data confirm that the different variants do not exhibit differential cytotoxicity and are consistent with previous evidences showing that Aβ42 (expressed alone or stabilized by the GFP tag) produced in the cytoplasm does not significantly impair yeast growth [29].

3.3. Solubility of Aβ42–GFP mutants in the yeast cytoplasm

In order to further characterize the aggregation properties of the different variants, yeast cells were lysed and the resulting soluble and insoluble fractions were analyzed by immunoblotting (Fig. 3A). Only the fusion proteins were immunoreactive to 6E10, an Aβ-specific antibody. Quantification of the bands corresponding to soluble and insoluble protein showed that, despite the presence of diffuse fluorescence in the cytosol and the absence of observable foci in many mutants, Aβ–GFP was in most cases mainly located in the insoluble fraction (Fig. 3B), a property that was independent of the system used for cell lysis and not caused by partial fractionation, since the endogenous yeast cyclin Clb2 and a recombinantly expressed GFP used as controls were localized exclusively in the soluble fraction (data not shown). This result is consistent with previous data in a similar yeast model, where Aβ42 was fused at the GFP C-terminus and in which both the wild type, forming cytoplasmic foci, and a double mutant Phe19Ser/Leu34Pro, displaying diffuse fluorescence, were found in the insoluble fraction [42]. However, in our conditions, the presence of soluble Aβ42–GFP was also observable for many of the mutants. This is in contrast to what was previously observed in *E. coli*, where, independent of the considered mutant, >95% of the protein was located in the insoluble fraction. To compare the solubility of the different variants in yeast, we normalized the fraction of insoluble protein relative to the sum of soluble and insoluble protein for each mutant (Fig. 3C). Consistent with their high intrinsic aggregation propensities, Phe, Trp, Ile and Tyr variants were almost exclusively located in the insoluble fractions while for polar residues like Glu, Asn

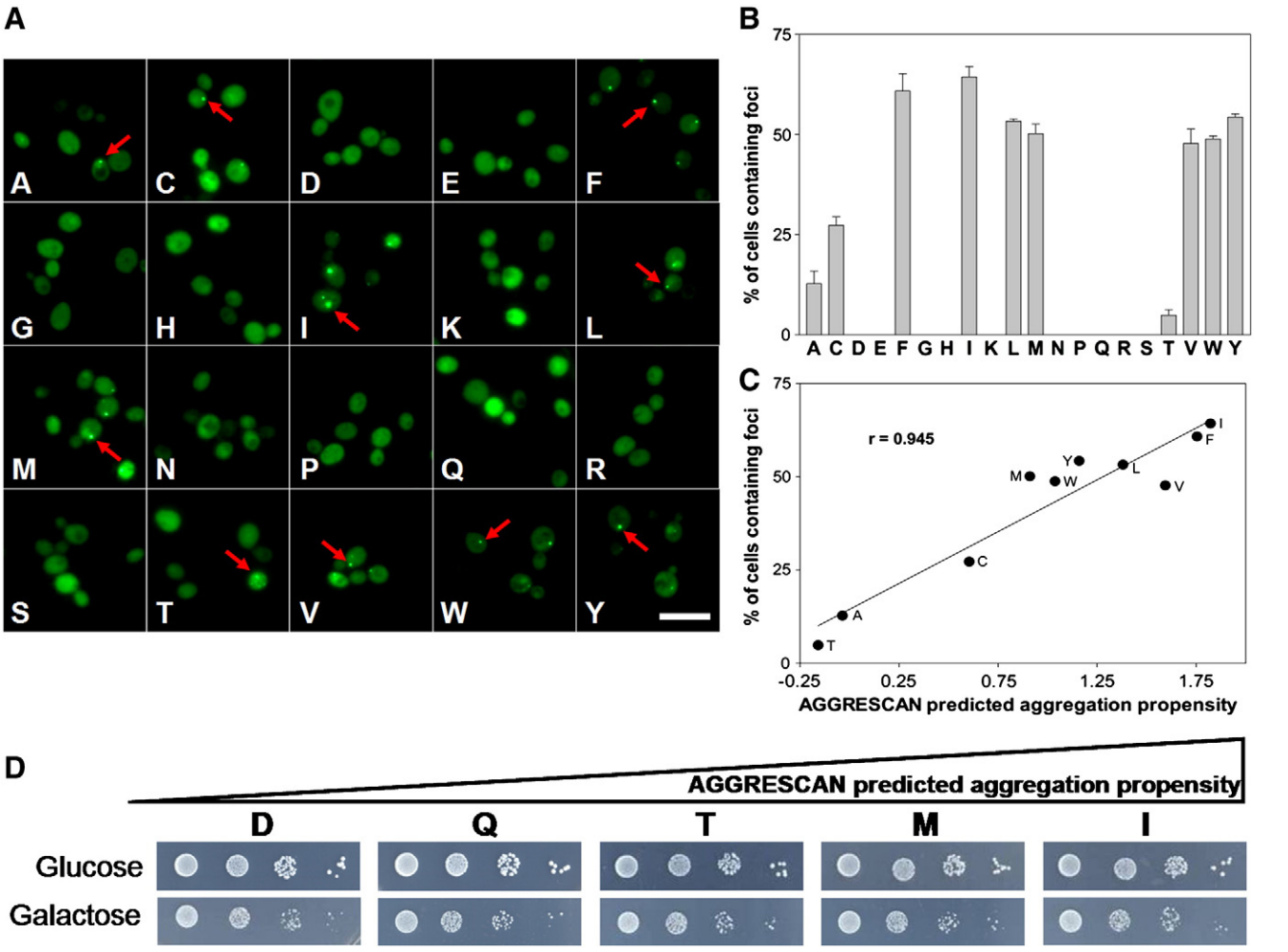

Fig. 2. Expression of the Aβ42–GFP mutants in the intracellular space of *S. cerevisiae*. (A) Microscopy images of yeast cells expressing Aβ42–GFP variants for 15 h under UV light. Fluorescence is present either as small foci (red arrows) or diffused in the cytoplasm of the cells. Scale bar represents 10 μm. (B) Graph bar representing the percentage of cells containing fluorescent foci for each mutant. Values were obtained by monitoring the number of cells with intracellular aggregates among ~1000 cells from two different cultures for each mutant. (C) Correlation between the percentage of cells containing visible intracellular aggregation foci and the intrinsic aggregation propensity predicted by AGGRESCAN. (D) Spotting assays in the presence of glucose and galactose (protein induction conditions) corresponding to 5 mutants expressing representative examples of Aβ42–GFP variants with different aggregation propensities.

and Gln, >40% of the protein fusion was located in the soluble fraction. A plot of the percentage of soluble protein present in each mutant relative to its AGGRESCAN predicted aggregation propensity renders a significant correlation ($R = 0.81$, $p < 0.00002$) suggesting that intrinsic properties are important determinants of the in vivo solubility of the mutants in the cytosol (Fig. 3C).

3.4. Fluorescence levels of Aβ42–GFP mutants in the yeast cytoplasm

In our protein fusions, the GFP moiety acts as a reporter of the aggregation state of Aβ42 [43]; thus the total fluorescence of intact cells was expected to reflect aggregation propensities, as it occurs in bacteria [20]. Fluorescence emission curves were collected for cells expressing each Aβ–GFP variant (representative examples are shown in Fig. 3D) and the relative intensity at the GFP emission maximum (510 nm) was measured (Fig. 3E). Again the aromatic residues Trp, Phe and Tyr displayed the lowest fluorescence levels and the polar residues Glu, Gln and Asn the highest, in such a way that the fluorescence emitted by cells expressing the Glu variant was nine-fold higher than that emitted by those expressing the Trp variant. This fluorescence dynamic range between the most and the least fluorescent mutant is more than two times higher than that observed in *E. coli*. Fluorescence emission and predicted aggregation propensity according to AGGRESCAN correlate significantly ($R = 0.78$ $p < 0.00003$) (Fig. 3F). However, an inspection of Fig. 3E and F allows to note deviations from the correlation for mutants bearing Trp and Phe, that, despite being predicted as aggregation-prone, behave as outliers, exhibiting lower levels of fluorescence emission than expected, which suggests that in contrast to bacteria, other factors apart from intrinsic aggregation propensity might influence the fate of Aβ–GFP proteins in the more complex yeast cytosol.

3.5. Protein levels of Aβ42–GFP mutants in the cytoplasm of yeast

From Fig. 4A it is evident that, apart from the distribution between the soluble and insoluble fraction, the mutants differ in the levels of total protein present in the cytosol. This is again in contrast with *E. coli* data, where protein levels were essentially identical between the different mutants [20]. To quantify the cytosolic protein levels we performed immunoblotting analysis with equal amounts of cells expressing the 20 different variants. As shown in Fig. 4A and B, striking differences between mutants were observed. Trp and Phe mutants display extremely low protein levels when compared with variants bearing polar residues like Glu or Gln. The correlation between expression levels and intrinsic aggregation propensity was significant but rather low ($R = 0.71$, $p < 0.0002$). Theoretically, a protein can fit into four different classes

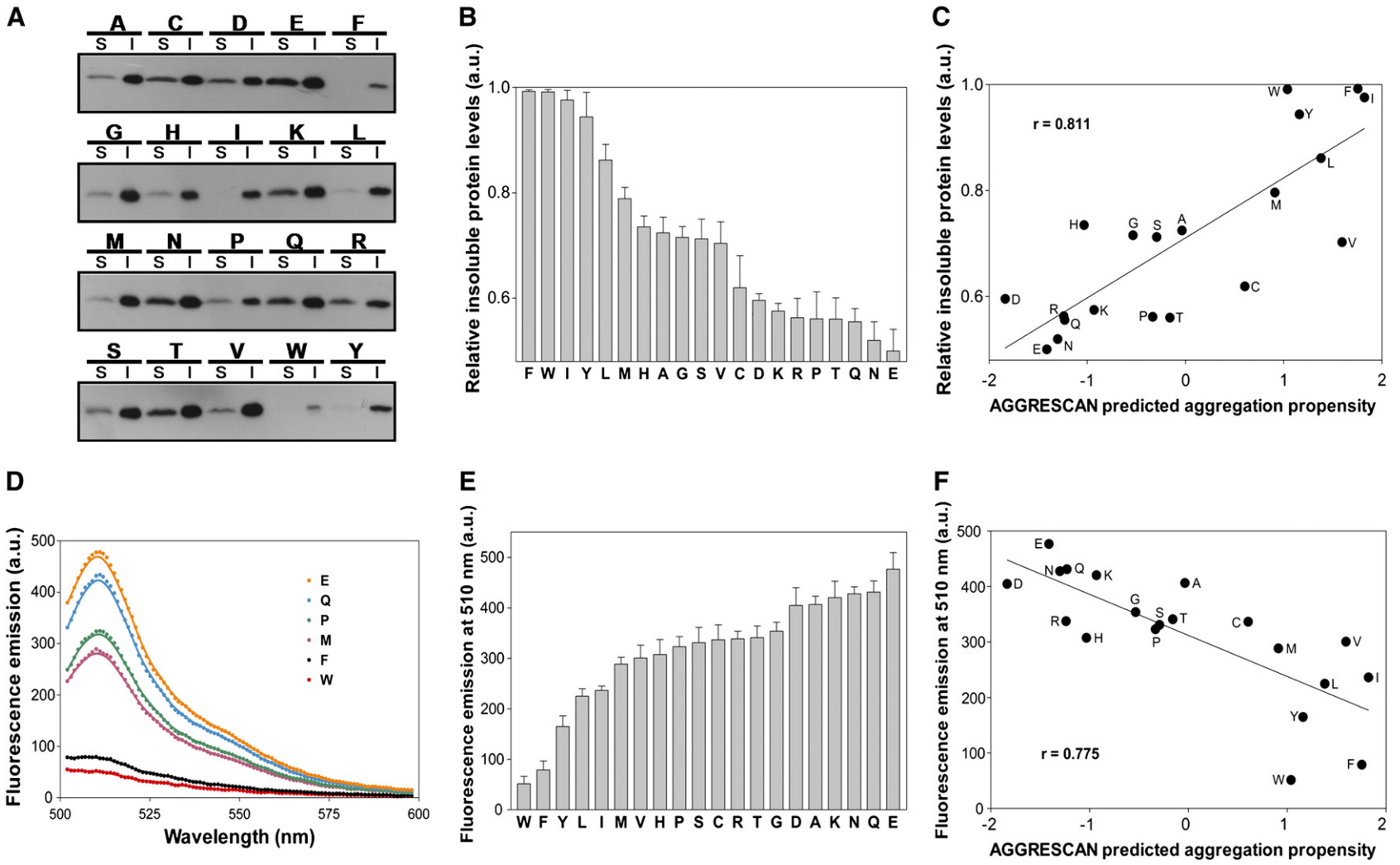

Fig. 3. Solubility and fluorescence of Aβ42–GFP mutants. (A) Western-blots of protein fractions for each mutant. Yeast cells were lysed with a chemical reagent and soluble and insoluble fractions were separated and loaded onto the protein gels. For each mutant: left and right bands correspond to the soluble (S) and insoluble (I) protein fractions, respectively. (B) Bar graph with the values obtained from the Western-blot quantification using ImageJ software. Each bar represents the ratio between insoluble and total protein levels. (C) Correlation between the relative amount of insoluble protein and the intrinsic aggregation propensity predicted by AGGRESCAN. (D) Examples of GFP fluorescence curves obtained from cultures after 15 h of expressing Aβ42–GFP. Emission curves of washed entire cells were recorded in a spectrofluorometer using an excitation wavelength of 488 nm. (E) Bar graph representing the fluorescence of the 20 mutants expressing Aβ42–GFP obtained from the GFP emission pick at 510 nm. (F) Correlation between the GFP fluorescence and the intrinsic aggregation propensity predicted by AGGRESCAN.

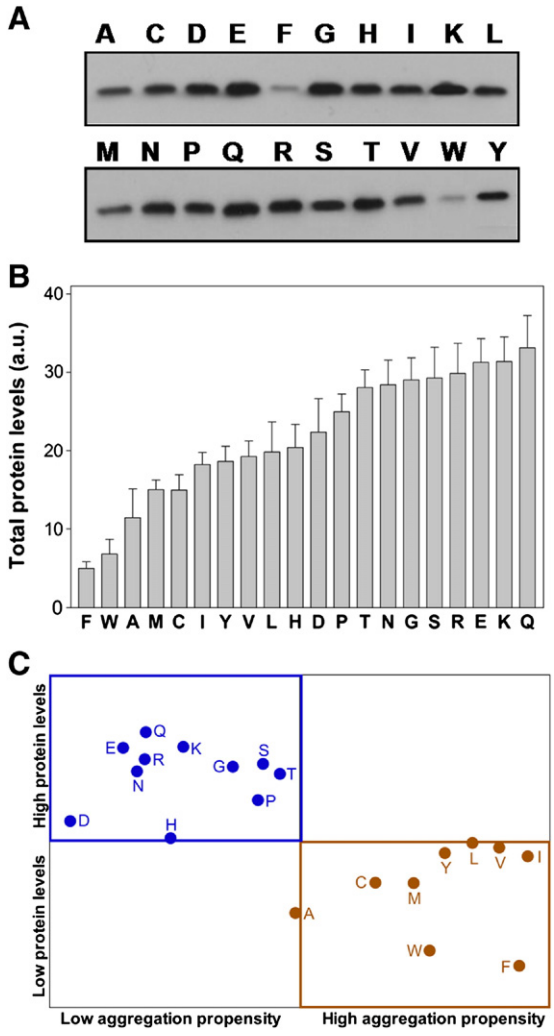

Fig. 4. Total Aβ42–GFP levels detected by immunoblotting. (A) Western-blots of the total protein fraction of each mutant. Equal amounts of cultures were loaded onto the protein gels, as well as a reference band (not shown) to compare both membranes. (B) Bar graph with the values obtained from the Western-blot quantification using ImageJ software. Each bar represents total AB42–GFP level. (C) Dot-plot representing the spatial distribution of Aβ42–GFP mutants depending on the intrinsic aggregation propensity predicted by AGGRESCAN and the amount of total Aβ42–GFP. In blue: mutants with low aggregation propensity (AGGRESCAN values <0) presenting high Aβ42–GFP levels. In red: mutants with high aggregation propensity (AGGRESCAN values >0) presenting low Aβ42–GFP levels.

depending on its aggregation propensity and relative protein levels (Fig. 4C). Interestingly, the Aβ–GFP protein set fits only into two of the four possible groups: (i) proteins with low aggregation propensity and high protein levels and (ii) proteins with high aggregation propensity and low protein levels. We did not observe any protein in the theoretical classes having high aggregation propensity and high protein levels or vice versa, which indicates that these two features are always anti-correlated in our protein set.

To ensure that the observed differences in protein levels were not caused by differential plasmid loss between mutants, and thus by differences in gene expression, cultures containing the same number of cells of Glu and Phe mutants were plated in glucose or galactose containing selective media 15 h after induction of protein expression and the number of resulting colonies quantified. No significant differences in the number of colonies generated by the two strains under repressing or inducing conditions were observed (Fig. S4) allowing to discard plasmid copy variability as a major contributor to the observed differences in protein levels.

3.6. Proteolytic clearance of Aβ42–GFP variants in yeast

Due to the often deleterious nature of aggregation-prone proteins, they are usually targeted to degradation to prevent their accumulation [44]. The ubiquitin–proteasome and autophagy–lysosome/vacuolar pathways are the two main routes of protein and organelle clearance in eukaryotic cells [45–47]. Differential proteolysis of the Aβ–GFP variants might well account for the observed differences in protein steady state levels. In yeast, amyloidogenic proteins can be degraded both by the proteasome and by autophagy/vacuolar systems [48,49]. Thus, we analyzed the impact of blocking these pathways, either using chemical compounds or genetically modified strains, on the levels of both the high and low aggregating Glu and Phe mutants.

We first addressed the role of autophagy by expressing the two Aβ–GFP fusions in a Δ*atg1* strain. The ATG1 gene (autophagy-specific gene 1) encodes for a serine/threonine kinase involved in autophagy regulation and essential for induction of the autophagic pathway [50]. After overnight expression, the amount of total protein was found to increase for both mutants, compared to parental strains, as revealed by immunoblotting (Fig. 5A). To further confirm that the autophagy/vacuolar pathways were involved in the degradation of these two proteins, they were expressed in the BJ5459 strain lacking the PEP4 gene encoding for the vacuolar protease proteinase A, which initiates the activation of different vacuolar hydrolases, including aminopeptidase I, carboxypeptidase Y and proteinase B [51]. As shown in Fig. 5A, the levels of the two proteins were higher in the mutant strain than in the parental one.

We used a chemical approach to further confirm the contribution of the autophagy/vacuolar pathways to the observed steady state protein levels. In this case, the cell wall permeable Δ*erg6* mutant yeast strain was used to facilitate drug uptake and increase the intracellular concentration of the drugs added to the culture [52]: PMSF and rapamycin. PMSF is a serine proteinase inhibitor that blocks the activity of numerous vacuolar proteases [53] without affecting the proteasome function. Rapamycin is an inhibitor of the Tor2 kinase, which negatively regulates the autophagic pathway; thus rapamycin acts as an autophagy-inducing drug [54]. Because these compounds are known to have pleiotropic effects in yeast cells, protein expression was arrested prior to pharmacological treatments. Immunoblotting analysis shows that for both mutants protein levels increase after PMSF treatment and are reduced after incubation with rapamycin, compared to the respective controls (Fig. 5B), confirming thus the role played by autophagy and vacuolar proteases in the degradation of these protein species.

We addressed the role of the proteasomal machinery in Aβ–GFP clearance using the potent proteasome inhibitor MG-132 [55] in the Δ*erg6* strain background. Immunoblots of MG-132 treated cells after arresting protein expression showed an increase in the protein levels of both mutants, when compared to controls (Fig. 5C), indicating that proteasome-mediated pathway is also involved in the processing of Aβ–GFP fusions.

Importantly, the changes in protein levels observed after chemical or genetic modulation of the different proteolytic pathways are not identical in the two mutants (Fig. 5D). Inhibition of proteolytic activity always has a higher impact on the levels of the Phe variant, whereas the induction of autophagy by rapamycin preferentially reduces the levels of the Glu mutant, likely because those of the Phe variant are already under autophagy control in normal conditions.

We hypothesized that the higher proteolytic susceptibility of the Phe mutant should be reflected not only in an overall lower protein levels in the cell population but also in a higher number of cells in which the protein has been completely degraded and thus fluorescence cannot be detected. To test this hypothesis, we compared the proportion of cells displaying and not displaying fluorescence in the Phe and Glu variants, as measured using flow cytometry, which allows to uncouple mean fluorescence emission and the number of cells in the population contributing to this fluorescence (Fig. 6). In agreement

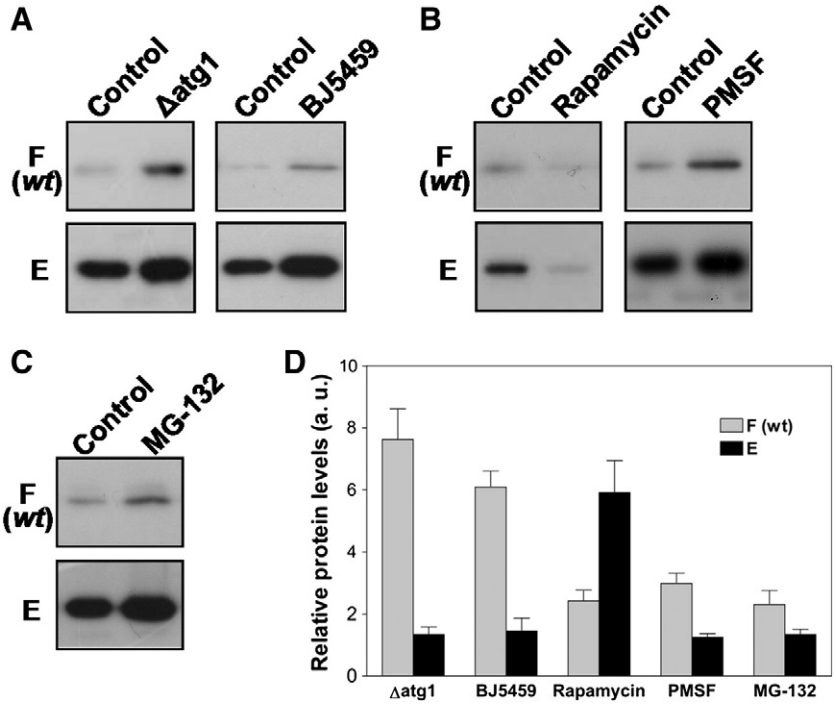

Fig. 5. Involvement of cellular proteolytic pathways affecting Aβ42–GFP levels in Aβ42–GFP*wt* (F) and Aβ42F19E–GFP (E) mutant. (A) Western-blots against Aβ42–GFP in the autophagy deficient Δ*atg1* strain (left) and in the protease deficient strain BJ5459 (right). Expression in BY4741 strain is used as control. (B) Western-blots against Aβ42–GFP in the wall-permeable strain Δ*erg6* in the presence of the autophagy enhancer rapamycin dissolved in DMSO (left) and in the presence of the proteases inhibitor PMSF dissolved in EtOH (right). Treatments with the corresponding solvents are used as controls. (C) Western-blots against Aβ42–GFP in the wall permeable strain Δ*erg6* in the presence of the proteasome inhibitor MG-132 dissolved in DMSO, which is used as control treatment. (D) Bar graph representing the variation in Aβ42–GFP levels caused by the genetic or chemical modulation of proteolytic pathways. Values are obtained from the quantification of Western-blots using ImageJ software and correspond to the ratio of protein after modulating the proteolytic activity and protein in their respective controls. In the case of rapamycin treatment, the inverse of the ratio is represented since this compound reduces the protein levels.

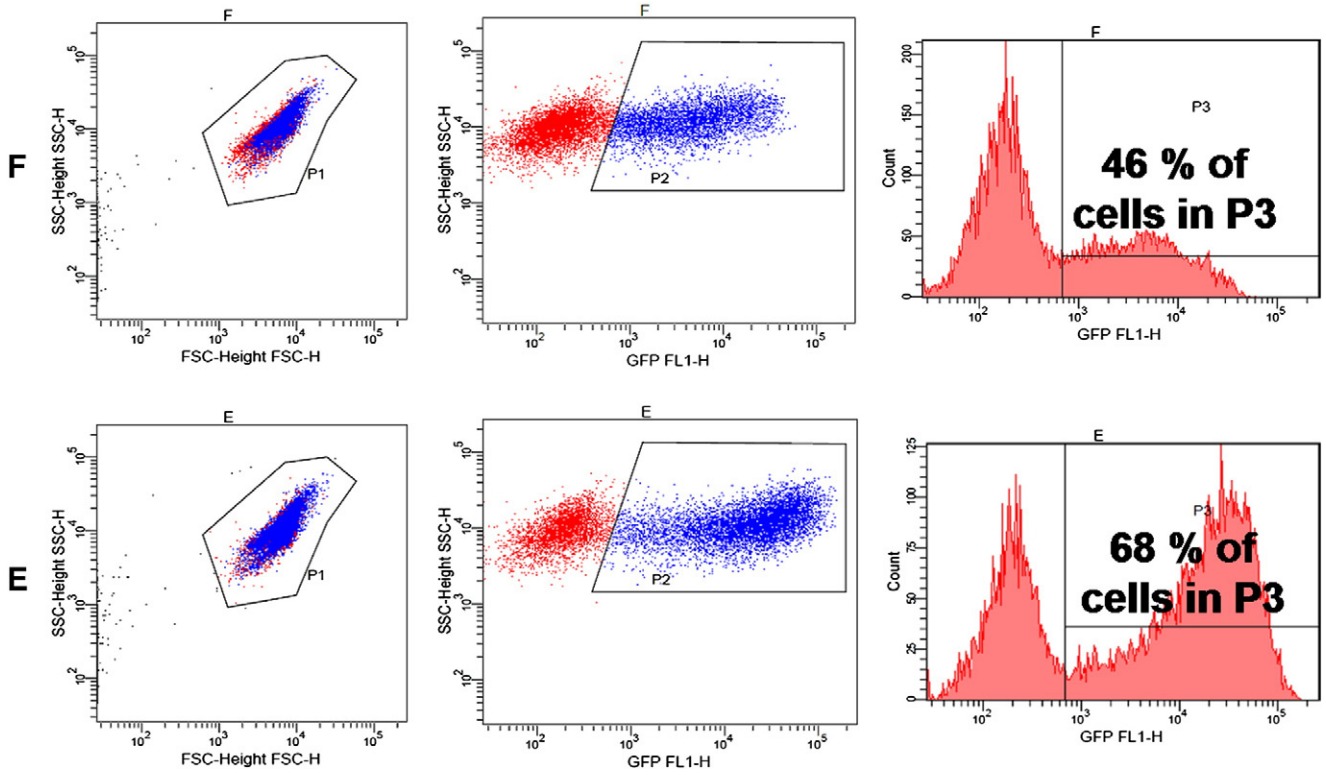

Fig. 6. Flow cytometry detection of cells expressing Aβ42–GFP. Flow cytometry analysis of F (*wt*) and E mutants (upper and lower series, respectively). Left panels correspond to forward scatter (FCS) vs. side scatter (SSC) dot-plots showing P1 gate. Middle panels correspond to SSC vs. GFP fluorescence dot-plots showing P2 population of cells expressing Aβ42–GFP. Right panels correspond to cell frequency histograms for the analysis of cells expressing Aβ42–GFP, delimited in P3 population. P2 and P3 are redundant populations exhibiting similar percentages.

with the spectrofluorimetric data, the mean fluorescence emission of cells expressing the Glu mutant was clearly higher than this of cells expressing the Phe variant. More interestingly, whereas we could detect fluorescence in 68% of Glu expressing cells, only 46% of Phe expressing cells exhibited fluorescence, suggesting a preferential action of the cellular proteolytic machinery against variants with high aggregation propensity and contributing to explain the association between aggregation propensity and protein levels observed in Fig. 4.

4. Discussion

Many late-onset neurodegenerative diseases are caused by aggregation-prone proteins [56]. Extensive genetic and transgenic data suggest that many of the mutations causing these proteinopathies trigger disease by conferring an increasing aggregation propensity to the affected proteins that results in a toxic gain of function [2]. The aggregation propensities of proteins are thought to be controlled to a large extent by the physicochemical properties encoded in the primary sequence [15]. It has been shown that this rule applies in vitro, however it is not clear that it will also work in vivo, where proteostatic mechanisms might introduce significant bias to this relationship. Thus, it is important to understand both the intrinsic properties and the pathways that regulate the fate of harmful aggregation-prone proteins inside living cells. In an attempt to provide new clues on this process, we have expressed in the yeast cytosol a library of 20 Aβ–GFP mutants exhibiting a continuous gradient of intrinsic aggregation propensities, as predicted by different algorithms (Fig. 1) and previously validated in vivo in bacteria [20]. The characterization of the aggregative properties of this protein set provides one of the few available quantitative data to model protein deposition inside eukaryotic cells.

A first important observation is that only half of the mutants formed detectable aggregated foci when expressed in yeast, indicating that in our particular experimental conditions it exits a threshold for intracellular inclusion formation. This contrasts with the data previously obtained in bacteria, where all the variants aggregated into inclusion bodies. In our set, the foci formation threshold is located between Ser and Thr, two polar uncharged residues differing only in a single methylene group, illustrating the exquisite control that the sequence exerts on in vivo aggregation propensities, especially if we take into account that the complete Aβ–GFP fusion consists of ~300 residues. In this way, if we only consider those variants for which foci formation could be observed, the correlation between the aggregation rates derived from *E. coli* experiments and the percentage of cells displaying inclusions in yeast is strikingly high, in such a way that the 10 mutants showing this capability match exactly with the 10 variants with the highest AGGRESCAN propensities, suggesting that, as it happens in bacteria [16], this algorithm constitutes a useful tool to predict protein aggregation tendencies in eukaryotic cells. The observed correlation between yeast and bacteria data provides one of the few experimental evidences that sequential features tune protein aggregation in a similar manner in different biological contexts, a concept that we all assume to be true when using aggregation predictors to forecast the impact of genetic mutations in human conformational disorders.

Although coherent with previous reports [42], it was surprising to observe that even for those mutants displaying only diffuse fluorescence, more than 50% of the recombinant protein was located in the insoluble fraction. This is consistent with the observation that in eukaryotic backgrounds, aggregation might be different from inclusion formation [57]. Inclusions refer to abnormal intracellular structures observed microscopically, while the formation of aggregates describes a biochemical phenomenon. The interchangeable use of the two terms results from the observation that aggregation-prone proteins linked to conformational disorders are often found in inclusions under pathological conditions. Our data indicate that in yeast these processes can be in fact experimentally dissociated. In eukaryotes the formation of inclusions is thought to be an active process involving different cellular components, including microtubules [58]. Accordingly, in a cellular model of HD it was shown that microtubule inhibition results in a marked reduction of inclusions, despite most of the poly-Q protein remained still aggregated [57]. However, this reduction of inclusion formation was also associated with an increase in the steady-state level of soluble protein, an observation that is coherent with the fact that mutants unable to form foci in our dataset are also those exhibiting the highest levels of soluble protein, thus linking protein-aggregation propensity and inclusion formation in yeast, in such a way that a certain level of solubility would likely prevent the proteins to enter the inclusion formation pathway. This is in contrast to what happens in bacteria, where formation of inclusions seems to depend on passive diffusion [59] and all Aβ–GFP variants, including those bearing polar residues in position 19, appear to be above the aggregation threshold; thus they differ in their kinetics of aggregation but not in their solubility at equilibrium [21].

Despite we find significant correlations between AGGRESCAN predicted aggregation propensities and the distribution of the variants in the soluble and insoluble fractions or their overall fluorescence emission, we also observe important deviations for certain mutants, which make both correlations being lower than expected. Specifically, the most aggregation-prone mutants tend to behave as outliers, displaying less soluble protein and fluorescence levels than predicted, which suggests that the fate of these mutants might be under special surveillance by the protein quality control machinery (PQC). The PQC consists of molecular chaperones and various proteases that recognize and repair damaged proteins or, alternatively, remove the aberrant proteins [60]. Although, these protein functions tend to be well conserved across species, the repertoire of proteins involved in PQC in bacteria and yeast is certainly divergent, which might contribute to the observed differences between *E. coli* and yeast models. The fact that, in contrast to bacteria, the protein steady levels differ between variants suggests that this is the case.

As a general trend, in our dataset proteins predicted to be soluble are present at higher levels than those with higher predicted aggregation propensity, in such a way that the cellular protein levels of the different mutants are anti-correlated with their intrinsic aggregation tendencies ($R = 0.71$, $p < 0.0002$). The aggregation propensity of a given protein sequence in a defined environment depends on different physicochemical properties, mainly on its hydrophobicity, secondary structure and overall change [15]. Zyggregator is an algorithm that uses a parameterization of these properties to predict aggregation propensities. The correlation between Zyggregator predictions and protein levels is however low ($R = 0.47$, $p < 0.02$), indicating that the specific parameters used to predict in vitro aggregation rates do not work properly to predict in vivo protein levels, which leads us to the question of what are the specific physicochemical properties recognized by the PQC resulting in different protein steady levels in our system (Fig. 7). In this context, charge does not seem to be a determinant factor, since Gln and Asn exhibit similar or higher protein levels than the charged acidic Glu and Asp residues. The secondary structure propensity of the polypeptide chain does not either seem to play a major role in PQC recognition, since the correlations of protein levels with β-sheet [61] ($R = 0.52$, $p < 0.009$) and α-helix [61] ($R = 0.24$, $p < 0.15$) propensities are rather low. This leaves us with hydrophobicity, a property known to be recognized by the yeast PQC in other protein models [62]. We selected hydrophobicity scales composed of experimentally determined transfer free energies for each individual amino acid since they include the contributions of the peptide bonds, an important feature if the protein region is expected to be unfolded and interacting with the components of the PQC. The correlation coefficients between protein levels and hydrophobicity are $R = 0.65$ ($p < 0.001$) and $R = 0.72$ ($p < 0.0002$) for the octanol [63] and interface [64] scales, respectively (Fig. 7). Thus, considering only the interface hydrophobicity of the residue at position 19 provides a predictive power similar to that of AGGRESCAN. In fact, Trp, the

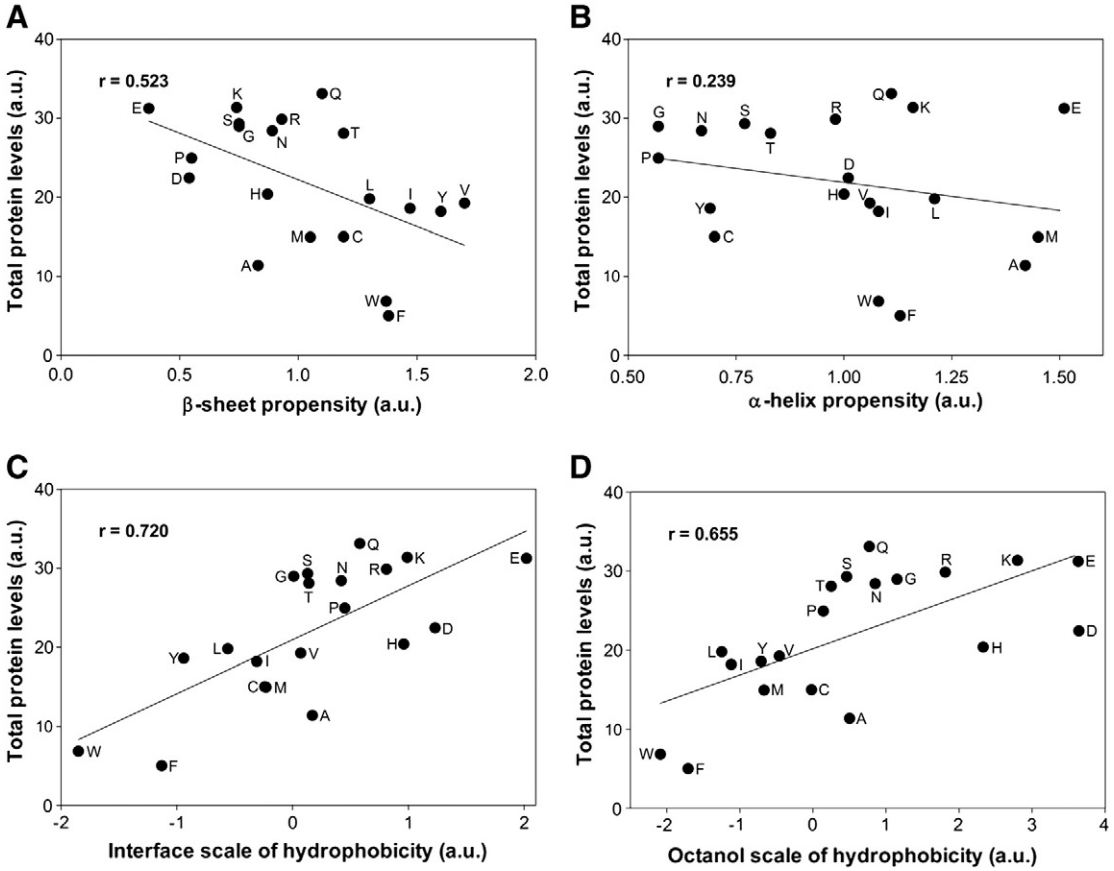

Fig. 7. Correlation between Aβ42–GFP protein levels and amino acid physicochemical properties. Aβ42–GFP total protein levels are plotted against different physiochemical properties of the residue in the 19th position for each mutant: (A) β-sheet propensity from the Chou & Fasman scale, (B) α-helix propensity from the Chou & Fasman scale, (C) hydrophobicity derived from the octanol scale and (D) hydrophobicity derived from the interface scale.

main outliner in the different plots, is the residue displaying the highest hydrophobicity in this scale.

The PQC degradation system should target misfolded species and not folded states, which implies that it needs to recognize a feature that reports selectively on conformational defects present in the misfolded state. Hydrophobicity fulfills this requirement better than secondary structure, which is characteristic of folded states, or charge, which is already exposed to solvent in native conformations. Exposed hydrophobicity constitutes in most cases a structural abnormality since hydrophobic residues are buried inside the core, involved in the formation of protein interfaces or located within membranes and, therefore, their exposure indicates defects in folding, assembly or membrane insertion. In our dataset, the mutated residues are expected to be located in an essentially disordered context and highly exposed to solvent, mimicking the conditions in a misfolded environment; thus our data provide strong support for a selective recognition of hydrophobicity by protein degradation systems. Accordingly, we show that autophagy/vacuolar pathways preferentially target wild type Aβ over the Glu mutant, since chemical or genetic inhibition of these pathways results in a higher relative increase of the protein levels in the wild type protein, whereas induction of autophagy has a more severe effect in the Glu variant; likely because under these specific conditions it becomes a substrate of the degradation pathway, whereas in normal conditions it is not. The same type of selectivity seems to apply for the proteasome mediated degradation of Aβ–GFP fusions. Interestingly enough, Phe, in the wild type, is the most hydrophobic residue in the interface scale after Trp, whereas Glu occupies the last position in this hydrophobicity ranking. The fact that both AGGRESCAN and hydrophobicity scales correlate similarly with protein levels suggests that the binding of protein substrates to PQC might require a degree of exposed hydrophobicity similar to that promoting self-assembly and aggregation of the substrates, allowing in this way the PQC to target specifically the degradation of dangerous insoluble sequences. This view is consistent with the fact that the binding sites of chaperones and ubiquitin ligases acting as upstream conformational sorters for degradative pathways are themselves hydrophobic [65,66].

Our results demonstrate that autophagy is involved in the clearance of wild type Aβ–GFP in yeast and are fully consistent with those recently reported for a C-terminal fusion of Aβ to GFP, where induction of autophagy by the drug latrepirdine resulted in an increased degradation [42], as well as with those obtained for a yeast model of α-synuclein aggregation [49], overall converging to point out autophagy as a critical and generic component of the cellular clearance of potentially toxic aggregation-prone proteins. Proteasomal degradation is also involved in the processing of Aβ–GFP, however its contribution is moderate and its activity cannot compensate for the lack of autophagic function since genetic or chemical inhibition of these pathways results in a much less efficient protein clearance when compared with wild type cells. In fact, it has been suggested that once aggregation-prone substrates cannot be efficiently handled by the proteasome, autophagy becomes the default clearance pathway [67]. Nevertheless, the aim of the present work is not to provide a detailed description of the pathways involved in intracellular Aβ–GFP degradation, but rather to demonstrate that the decision on whether a substrate would become a target or not of these pathways depends on its intrinsic aggregation/hydrophobicity propensity. Flow cytometry data indicate that the PQC performs fairly well in protecting cells from the presence aggregation-prone wild type Aβ–GFP variant, since less than half of the cells exhibit detectable fluorescence and thus an intact fusion, consistent with the view that a robust

PQC degradation system should target those misfolded species with a higher risk of forming insoluble aggregates. Nevertheless, in agreement with previous observations [29,41], aggregation-prone mutants forming intracellular deposits are not more cytotoxic than those displaying diffuse cytosolic fluorescence. This might indicate that moderate amounts of Aβ–GFP aggregates would be below a threshold for toxicity in yeast, as previously suggested for α-synuclein [49], or, alternatively, they might play a cytoprotective role as shown for mammalian aggresomes, which serve as cytoplasmic recruitment centers to facilitate degradation of toxic proteins by autophagic pathways [57]. If this latter scenario also applies in yeast, it would be consistent with our observation that the most aggregation-prone variants both form inclusions and are preferentially targeted for protein degradation, since these two outcomes would respond to the same process.

It is clear that a deeper knowledge of the mechanism by which proteins are targeted for degradation will be important for understanding pathologic processes. Our present demonstration that sorting to these pathways is strongly influenced by the physicochemical properties of the protein sequence should facilitate the development of rational therapeutic approaches for protein conformational diseases. The potency of these types of strategies is highlighted by the recent observation that proteins 'tagged' with small, synthetic, non-polar molecules that increase their surface hydrophobicity, a key property according to our study, are targeted for degradation by the PQC, allowing thus their selective removal [68].

Supplementary data to this article can be found online at http://dx.doi.org/10.1016/j.bbamcr.2013.06.023.

Acknowledgements

We thank Dr. Josep A. Biosca (Universitat Autònoma de Barcelona) for kindly providing us the BJ5459 yeast strain as well as Prof. Gerhard H. Braus (Georg-August-Universität Göttingen) for the Δ*erg6* and Δ*atg1* yeast strains. Work in our lab is supported by grants BFU2010-14901 from the Ministerio de Ciencia e Innovación (Spain) and 2009-SGR 760 from the AGAUR (Generalitat de Catalunya). SV has been granted an ICREA ACADEMIA award (ICREA).

References

[1] F. Chiti, C.M. Dobson, Protein misfolding, functional amyloid, and human disease, Annu. Rev. Biochem. 75 (2006) 333–366.
[2] G. Invernizzi, E. Papaleo, R. Sabate, S. Ventura, Protein aggregation: mechanisms and functional consequences, Int. J. Biochem. Cell Biol. 44 (2012) 1541–1554.
[3] M. Morell, N.S. de Groot, J. Vendrell, F.X. Aviles, S. Ventura, Linking amyloid protein aggregation and yeast survival, Mol. Biosyst. 7 (2011) 1121–1128.
[4] S. Ventura, A. Villaverde, Protein quality in bacterial inclusion bodies, Trends Biotechnol. 24 (2006) 179–185.
[5] M. Carrio, N. Gonzalez-Montalban, A. Vera, A. Villaverde, S. Ventura, Amyloid-like properties of bacterial inclusion bodies, J. Mol. Biol. 347 (2005) 1025–1037.
[6] L. Wang, S.K. Maji, M.R. Sawaya, D. Eisenberg, R. Riek, Bacterial inclusion bodies contain amyloid-like structure, PLoS Biol. 6 (2008) e195.
[7] M. Morell, R. Bravo, A. Espargaro, X. Sisquella, F.X. Aviles, X. Fernandez-Busquets, S. Ventura, Inclusion bodies: specificity in their aggregation process and amyloid-like structure, Biochim. Biophys. Acta 1783 (2008) 1815–1825.
[8] C.M. Dobson, The structural basis of protein folding and its links with human disease, Philos. Trans. R. Soc. Lond. B Biol. Sci. 356 (2001) 133–145.
[9] F. Rousseau, J. Schymkowitz, L. Serrano, Protein aggregation and amyloidosis: confusion of the kinds? Curr. Opin. Struct. Biol. 16 (2006) 118–126.
[10] A.W. Fitzpatrick, T.P. Knowles, C.A. Waudby, M. Vendruscolo, C.M. Dobson, Inversion of the balance between hydrophobic and hydrogen bonding interactions in protein folding and aggregation, PLoS Comput. Biol. 7 (2011) e1002169.
[11] R. Linding, J. Schymkowitz, F. Rousseau, F. Diella, L. Serrano, A comparative study of the relationship between protein structure and beta-aggregation in globular and intrinsically disordered proteins, J. Mol. Biol. 342 (2004) 345–353.
[12] A. Espargaro, V. Castillo, N.S. de Groot, S. Ventura, The in vivo and in vitro aggregation properties of globular proteins correlate with their conformational stability: the SH3 case, J. Mol. Biol. 378 (2008) 1116–1131.
[13] S. Ventura, Sequence determinants of protein aggregation: tools to increase protein solubility, Microb. Cell Factories 4 (2005) 11.
[14] S. Ventura, J. Zurdo, S. Narayanan, M. Parreno, R. Mangues, B. Reif, F. Chiti, E. Giannoni, C.M. Dobson, F.X. Aviles, L. Serrano, Short amino acid stretches can mediate amyloid formation in globular proteins: the Src homology 3 (SH3) case, Proc. Natl. Acad. Sci. U. S. A. 101 (2004) 7258–7263.
[15] F. Chiti, M. Stefani, N. Taddei, G. Ramponi, C.M. Dobson, Rationalization of the effects of mutations on peptide and protein aggregation rates, Nature 424 (2003) 805–808.
[16] M. Belli, M. Ramazzotti, F. Chiti, Prediction of amyloid aggregation in vivo, EMBO Rep. 12 (2011) 657–663.
[17] V. Castillo, R. Grana-Montes, R. Sabate, S. Ventura, Prediction of the aggregation propensity of proteins from the primary sequence: aggregation properties of proteomes, Biotechnol. J. 6 (2011) 674–685.
[18] A.B. Ahmed, A.V. Kajava, Breaking the amyloidogenicity code: methods to predict amyloids from amino acid sequence, FEBS Lett. 587 (2013) 1089–1095.
[19] D. Guidolin, L.F. Agnati, G. Albertin, C. Tortorella, K. Fuxe, Bioinformatics aggregation predictors in the study of protein conformational diseases of the human nervous system, Electrophoresis 33 (2012) 3669–3679.
[20] N.S. de Groot, F.X. Aviles, J. Vendrell, S. Ventura, Mutagenesis of the central hydrophobic cluster in Abeta42 Alzheimer's peptide. Side-chain properties correlate with aggregation propensities, FEBS J. 273 (2006) 658–668.
[21] N.S. de Groot, S. Ventura, Protein activity in bacterial inclusion bodies correlates with predicted aggregation rates, J. Biotechnol. 125 (2006) 110–113.
[22] O. Conchillo-Sole, N.S. de Groot, F.X. Aviles, J. Vendrell, X. Daura, S. Ventura, AGGRESCAN: a server for the prediction and evaluation of "hot spots" of aggregation in polypeptides, BMC Bioinforma. 8 (2007) 65.
[23] N.S. de Groot, V. Castillo, R. Grana-Montes, S. Ventura, AGGRESCAN: method, application, and perspectives for drug design, Methods Mol. Biol. 819 (2012) 199–220.
[24] A. Espargaro, R. Sabate, S. Ventura, Kinetic and thermodynamic stability of bacterial intracellular aggregates, FEBS Lett. 582 (2008) 3669–3673.
[25] A. Villar-Pique, N.S. de Groot, R. Sabate, S.P. Acebron, G. Celaya, X. Fernandez-Busquets, A. Muga, S. Ventura, The effect of amyloidogenic peptides on bacterial aging correlates with their intrinsic aggregation propensity, J. Mol. Biol. 421 (2012) 270–281.
[26] V. Khurana, S. Lindquist, Modelling neurodegeneration in *Saccharomyces cerevisiae*: why cook with baker's yeast? Nat. Rev. Neurosci. 11 (2010) 436–449.
[27] S. Tenreiro, T.F. Outeiro, Simple is good: yeast models of neurodegeneration, FEMS Yeast Res. 10 (2010) 970–979.
[28] S. Treusch, S. Hamamichi, J.L. Goodman, K.E. Matlack, C.Y. Chung, V. Baru, J.M. Shulman, A. Parrado, B.J. Bevis, J.S. Valastyan, H. Han, M. Lindhagen-Persson, E.M. Reiman, D.A. Evans, D.A. Bennett, A. Olofsson, P.L. DeJager, R.E. Tanzi, K.A. Caldwell, G.A. Caldwell, S. Lindquist, Functional links between Abeta toxicity, endocytic trafficking, and Alzheimer's disease risk factors in yeast, Science 334 (2011) 1241–1245.
[29] F. D'Angelo, H. Vignaud, J. Di Martino, B. Salin, A. Devin, C. Cullin, C. Marchal, A yeast model for amyloid-beta aggregation exemplifies the role of membrane trafficking and PICALM in cytotoxicity, Dis. Model. Mech. 6 (2013) 206–216.
[30] A.A. Cooper, A.D. Gitler, A. Cashikar, C.M. Haynes, K.J. Hill, B. Bhullar, K. Liu, K. Xu, K.E. Strathearn, F. Liu, S. Cao, K.A. Caldwell, G.A. Caldwell, G. Marsischky, R.D. Kolodner, J. Labaer, J.C. Rochet, N.M. Bonini, S. Lindquist, Alpha-synuclein blocks ER-Golgi traffic and Rab1 rescues neuron loss in Parkinson's models, Science 313 (2006) 324–328.
[31] T.F. Outeiro, S. Lindquist, Yeast cells provide insight into alpha-synuclein biology and pathobiology, Science 302 (2003) 1772–1775.
[32] S. Krobitsch, S. Lindquist, Aggregation of huntingtin in yeast varies with the length of the polyglutamine expansion and the expression of chaperone proteins, Proc. Natl. Acad. Sci. U. S. A. 97 (2000) 1589–1594.
[33] S. Willingham, T.F. Outeiro, M.J. DeVit, S.L. Lindquist, P.J. Muchowski, Yeast genes that enhance the toxicity of a mutant huntingtin fragment or alpha-synuclein, Science 302 (2003) 1769–1772.
[34] S. Tenreiro, M.C. Munder, S. Alberti, T.F. Outeiro, Harnessing the power of yeast to unravel the molecular basis of neurodegeneration, J. Neurochem. (2013), http://dx.doi.org/10.1111/jnc.1227.
[35] E.W. Jones, Tackling the protease problem in *Saccharomyces cerevisiae*, Methods Enzymol. 194 (1991) 428–453.
[36] A. Morimoto, K. Irie, K. Murakami, Y. Masuda, H. Ohigashi, M. Nagao, H. Fukuda, T. Shimizu, T. Shirasawa, Analysis of the secondary structure of beta-amyloid (Abeta42) fibrils by systematic proline replacement, J. Biol. Chem. 279 (2004) 52781–52788.
[37] G. Bitan, S.S. Vollers, D.B. Teplow, Elucidation of primary structure elements controlling early amyloid beta-protein oligomerization, J. Biol. Chem. 278 (2003) 34882–34889.
[38] G.G. Tartaglia, M. Vendruscolo, The Zyggregator method for predicting protein aggregation propensities, Chem. Soc. Rev. 37 (2008) 1395–1401.
[39] S.O. Garbuzynskiy, M.Y. Lobanov, O.V. Galzitskaya, FoldAmyloid: a method of prediction of amyloidogenic regions from protein sequence, Bioinformatics 26 (2010) 326–332.
[40] A.M. Fernandez-Escamilla, F. Rousseau, J. Schymkowitz, L. Serrano, Prediction of sequence-dependent and mutational effects on the aggregation of peptides and proteins, Nat. Biotechnol. 22 (2004) 1302–1306.
[41] S. Bagriantsev, S. Liebman, Modulation of Abeta42 low-n oligomerization using a novel yeast reporter system, BMC Biol. 4 (2006) 32.
[42] P.R. Bharadwaj, G. Verdile, R.K. Barr, V. Gupta, J.W. Steele, M.L. Lachenmayer, Z. Yue, M.E. Ehrlich, G. Petsko, S. Ju, D. Ringe, S.E. Sankovich, J.M. Caine, I.G. Macreadie, S. Gandy, R.N. Martins, Latrepirdine (Dimebon) enhances autophagy and reduces intracellular GFP-Abeta42 levels in yeast, J. Alzheimers Dis. 32 (2012) 949–967.
[43] A. Villar-Pique, A. Espargaro, R. Sabate, N.S. de Groot, S. Ventura, Using bacterial inclusion bodies to screen for amyloid aggregation inhibitors, Microb. Cell Factories 11 (2012) 55.
[44] D.C. Rubinsztein, The roles of intracellular protein-degradation pathways in neurodegeneration, Nature 443 (2006) 780–786.

[45] K. Tanaka, T. Mizushima, Y. Saeki, The proteasome: molecular machinery and pathophysiological roles, Biol. Chem. 393 (2012) 217–234.
[46] J.L. Webb, B. Ravikumar, J. Atkins, J.N. Skepper, D.C. Rubinsztein, Alpha-synuclein is degraded by both autophagy and the proteasome, J. Biol. Chem. 278 (2003) 25009–25013.
[47] D.C. Rubinsztein, P. Codogno, B. Levine, Autophagy modulation as a potential therapeutic target for diverse diseases, Nat. Rev. Drug Discov. 11 (2012) 709–730.
[48] D. Kaganovich, R. Kopito, J. Frydman, Misfolded proteins partition between two distinct quality control compartments, Nature 454 (2008) 1088–1095.
[49] D. Petroi, B. Popova, N. Taheri-Talesh, S. Irniger, H. Shahpasandzadeh, M. Zweckstetter, T.F. Outeiro, G.H. Braus, Aggregate clearance of alpha-synuclein in *Saccharomyces cerevisiae* depends more on autophagosome and vacuole function than on the proteasome, J. Biol. Chem. 287 (2012) 27567–27579.
[50] A. Matsuura, M. Tsukada, Y. Wada, Y. Ohsumi, Apg1p, a novel protein kinase required for the autophagic process in *Saccharomyces cerevisiae*, Gene 192 (1997) 245–250.
[51] C.A. Woolford, L.B. Daniels, F.J. Park, E.W. Jones, J.N. Van Arsdell, M.A. Innis, The PEP4 gene encodes an aspartyl protease implicated in the posttranslational regulation of *Saccharomyces cerevisiae* vacuolar hydrolases, Mol. Cell. Biol. 6 (1986) 2500–2510.
[52] R. Emter, A. Heese-Peck, A. Kralli, ERG6 and PDR5 regulate small lipophilic drug accumulation in yeast cells via distinct mechanisms, FEBS Lett. 521 (2002) 57–61.
[53] E.W. Jones, Vacuolar proteases and proteolytic artifacts in *Saccharomyces cerevisiae*, Methods Enzymol. 351 (2002) 127–150.
[54] Y. Kamada, T. Sekito, Y. Ohsumi, Autophagy in yeast: a TOR-mediated response to nutrient starvation, Curr. Top. Microbiol. Immunol. 279 (2004) 73–84.
[55] D.H. Lee, A.L. Goldberg, Proteasome inhibitors: valuable new tools for cell biologists, Trends Cell Biol. 8 (1998) 397–403.
[56] C.M. Dobson, Protein-misfolding diseases: getting out of shape, Nature 418 (2002) 729–730.
[57] J.P. Taylor, F. Tanaka, J. Robitschek, C.M. Sandoval, A. Taye, S. Markovic-Plese, K.H. Fischbeck, Aggresomes protect cells by enhancing the degradation of toxic polyglutamine-containing protein, Hum. Mol. Genet. 12 (2003) 749–757.
[58] R.R. Kopito, Aggresomes, inclusion bodies and protein aggregation, Trends Cell Biol. 10 (2000) 524–530.
[59] A.S. Coquel, J.P. Jacob, M. Primet, A. Demarez, M. Dimiccoli, T. Julou, L. Moisan, A.B. Lindner, H. Berry, Localization of protein aggregation in *Escherichia coli* is governed by diffusion and nucleoid macromolecular crowding effect, PLoS Comput. Biol. 9 (2013) e1003038.
[60] B. Chen, M. Retzlaff, T. Roos, J. Frydman, Cellular strategies of protein quality control, Cold Spring Harb. Perspect. Biol. 3 (2011) a004374.
[61] P.Y. Chou, G.D. Fasman, Conformational parameters for amino acids in helical, beta-sheet, and random coil regions calculated from proteins, Biochemistry 13 (1974) 211–222.
[62] E.K. Fredrickson, J.C. Rosenbaum, M.N. Locke, T.I. Milac, R.G. Gardner, Exposed hydrophobicity is a key determinant of nuclear quality control degradation, Mol. Biol. Cell 22 (2011) 2384–2395.
[63] W.C. Wimley, T.P. Creamer, S.H. White, Solvation energies of amino acid side chains and backbone in a family of host–guest pentapeptides, Biochemistry 35 (1996) 5109–5124.
[64] W.C. Wimley, S.H. White, Experimentally determined hydrophobicity scale for proteins at membrane interfaces, Nat. Struct. Biol. 3 (1996) 842–848.
[65] X. Zhu, X. Zhao, W.F. Burkholder, A. Gragerov, C.M. Ogata, M.E. Gottesman, W.A. Hendrickson, Structural analysis of substrate binding by the molecular chaperone DnaK, Science 272 (1996) 1606–1614.
[66] E.K. Fredrickson, R.G. Gardner, Selective destruction of abnormal proteins by ubiquitin-mediated protein quality control degradation, Semin. Cell Dev. Biol. 23 (2012) 530–537.
[67] H.J. Rideout, I. Lang-Rollin, L. Stefanis, Involvement of macroautophagy in the dissolution of neuronal inclusions, Int. J. Biochem. Cell Biol. 36 (2004) 2551–2562.
[68] T.K. Neklesa, C.M. Crews, Chemical biology: greasy tags for protein removal, Nature 487 (2012) 308–309.